RESEARCH ARTICLE

Phosphorus adsorption on natural sediments with different pH incorporating surface morphology characterization

Lei Huang[1] · Hongwei Fang[1] · Guojian He[1] · Minghong Chen[2]

Abstract Sediment samples from University Lake (U.L.) and Anacostia River (A.R.) were collected to study the phosphorus (P) adsorption with pH at 3.65, 4.75, and 5.65. The surface micro-morphology and pore structures of sediment particles were obtained using a scanning electron microscopy and gas adsorption method, respectively. Fourier analysis was then applied to approximate the surface morphology, which was incorporated into the Langmuir isotherm to directly derive the model parameters for P adsorption simulation. Meanwhile, an empirical function of pH was introduced to represent the pH effect on P adsorption. A stronger P adsorption was observed for the A.R. sediment due to the more clay minerals, smaller median diameter, and a greater percentage of large pores, and the increasing pH resulted in a decrease of adsorption equilibrium constant as well as the P adsorption capacity, which was well reproduced by the adsorption isotherms. This study would benefit the mechanism study of the interactions between sediment particles and pollutants, providing references for understanding the pollutants' transport in aqueous systems.

✉ Hongwei Fang
  fanghw@tsinghua.edu.cn

1 State Key Laboratory of Hydro-Science and Engineering, Department of Hydraulic Engineering, Tsinghua University, Beijing 100084, China

2 College of Water Resources and Civil Engineering, China Agricultural University, Beijing 100083, China

Introduction

There are various pollutants existing in natural waters, such as nutrients, heavy metals, and organics, and the fate and transport of pollutants significantly affect water quality conditions of the aqueous systems (Iqbal et al. 2015). Sediment particles, the important carrier of pollutants, have a strong affinity to pollutants due to their great specific surface areas and active surface sites (Davis and Kent 1990; Wang et al. 2009). Most pollutants in waters are adsorbed by sediment particles, and sediment dynamics play a crucial role on the pollutants' transport (Huang et al. 2015; Iqbal et al. 2015). Therefore, understanding the adsorption mechanisms of sediment particles can strongly improve the knowledge on the fate and transport of pollutants, potentially guiding risk assessments and the design of remediation strategies.

Adsorption is the accumulation of substances at the interfaces, e.g., solid/liquid interface (Brandt et al. 1993). It is an extremely complex phenomena affected by different factors. In recent decades, a great number of studies have been carried out to explore the mechanisms of adsorption, and the effects of various extrinsic/intrinsic factors have been extensively investigated, e.g., pH value (Antelo et al. 2005; Palleyi et al. 2015), ion strength (Wang et al. 2006; Zhao et al. 2015) and temperature (Johnson 1990; Rodda et al. 1996), particle size (Selig 2003; Han et al. 2008), mineral composition (Yu et al. 2001; Wang et al. 2012; Venkatramanan et al. 2015), etc. Knowledge about the adsorption mechanisms has been evidently improved. However, the effects of surface morphology on pollutants' adsorption have rarely been reported. Most natural sediment particles have extremely complex surface

morphology and numerous pores of various dimensions due to the diagenetic and transport processes, which influence the interactions between sediment particles and pollutants, and facilitate the pollutants' adsorption significantly (Fang et al. 2008, 2015).

Phosphorus (P), one of the key nutrients affecting water quality, is the major limiting factor for eutrophication (Schindler 2006; Elser et al. 2007). Studies show that particulate P is the major contributor of the P loading in the Yangtze River (Shen 2006), indicating the significant interactions between sediment particles and phosphate ions. In previous studies, Fang et al. (2013) conducted batch P adsorption experiments and measured the distribution of adsorbed P at different surface micro-morphologies (such as peak, ridge, channel, pass, pit, and slope) using energy dispersive X-ray spectroscopy. Statistics showed that adsorbed P mostly existed in the ridge and channel regions, with a few in the slope region, and casually in the peak, pass, and pit regions. The P adsorption on the surface of a mathematical sediment particle was then simulated by Fang et al. (2014) based on the statistical results of measured P distribution, providing a novel method to explore the relation between sediment and phosphate.

In this study, the effects of surface morphology on the adsorption properties of natural sediment particles were further explored to integrate the surface morphology and macro-level adsorption properties. Langmuir isotherm is the most common adsorption isotherm for solid/liquid systems, and many mathematical methods have been applied to determine the model parameters including linear and non-linear optimization regressions (Yan et al. 2015; Fang et al. 2016). Here, we characterized the surface properties of sediment particles using a scanning electron microscopy and gas adsorption method, including the surface micro-morphology and pore structures, which were incorporated into the Langmuir isotherm to directly derive the model parameters for adsorption simulation. Then, the P adsorption was investigated with different pH values. These results would enhance our understanding of the interactions between sediment particles and pollutants, which would improve the knowledge on the fate and transport of pollutants in aqueous systems.

Materials and methods

Sampling and analyses

Sediment samples in this study were collected from University Lake (U.L.) and Anacostia River (A.R.). The University Lake is a small freshwater lake located in the campus of Louisiana State University. The Anacostia River (Washington, D.C.) is a freshwater watershed located within the Potomac River drainage basin, which discharges to the Chesapeake Bay (Hong et al. 2011). Surficial sediment samples were collected using a core sampling device, and stored in pre-cleaned polyethylene bags at 4 °C until arriving at the laboratory. In the laboratory, the sediments were air-dried, ground, and passed through a 125-μm sieve to remove the impurities.

X-ray diffraction analysis was performed to obtain the mineral composition of the sediments (Dmax-RB 12 kW, Rigaku, Japan). The grain size of the sediments was measured using a laser scattering particle size distribution analyzer (LA-920, Horiba, Japan), and was classified into three fractions: clay (<0.004 mm), silt (0.004–0.062 mm), and sand fractions (0.062–2 mm). A scanning electron microscopy (JEOL JSM-6310F) was employed to analyze the surface morphology and microstructure of the sediments. The pore structures, including the pore volume and pore size distribution, were characterized by gas adsorption process (Autosorb-1-C, Quantachrome Instruments Inc., USA) and analyzed through the Barrett-Joyner-Halenda (BJH) theory (Barrett et al. 1951).

Adsorption isotherms

Phosphorus (P) adsorption experiments were carried out with three different pH values (i.e., 3.65,[1] 4.75, and 5.65) by adding sodium acetate-acetic acid buffer. Samples of 0.1, 0.2, 0.4, 0.8, 1.0, 1.5, and 2.0 g dried sediments were loaded into a series of 50-mL polypropylene centrifuge tubes with 30 mL of phosphate solution (15 mg P/L anhydrous KH_2PO_4 with the background electrolyte of 0.01 M $NaNO_3$). After shaking at room temperature for 24 h, the tubes were centrifuged, and the supernatant were filtered through 0.45-μm membrane. Then, the P concentrations were analyzed using the ammonium molybdate spectrophotometric method. The adsorbed P was calculated from the difference between the concentrations before and after equilibrium with sediment. In the experiments, triplicates were carried out, and the data were expressed as the average ± standard deviation in the following sections. The P adsorption isotherm can be fitted using the Langmuir model (Olsen and Watanabe 1957; Hao et al. 2003):

$$Q = Q_{max} \frac{KC}{1 + KC}, \tag{1}$$

where Q is the amount of P adsorbed per gram of sediment at equilibrium (mg/g), Q_{max} is the maximum possible amount of P adsorbed per gram of sediment (mg/g), K is the adsorption equilibrium constant related to the affinity of sediment particles to phosphate ions (L/mg), and C is the aqueous P concentration at equilibrium (mg/L). Generally, the parameters Q_{max} and K were determined using the linear or non-linear optimization regressions (Yan et al. 2015). Here, the adsorption capacity Q_{max} (mg/g) was calculated as a steric close-packed

---

[1] At pH 3.65, samples of 1.0 g dried sediments were loaded into a series of 30-mL phosphate solutions with the P concentrations of 1.0, 2.0, 5.0, 10, 20, 25, and 30 mg/L.

layer of the adsorbed phosphate ions, i.e., an ideal maximum P adsorption capacity, which depended on the complex surface morphology of sediment samples and the packing area of the adsorbed ion. An average packing area of 0.6 nm^2 for the adsorbed phosphate ions was proposed by Goldberg and Sposito (1984) and applied in this study. The adsorption equilibrium constant K was calculated from only the coulombic energy (Hao et al. 2003),

$$K = \exp\left(\frac{-\Delta G_{coul}}{RT}\right) = \exp\left(\frac{-zF_x}{RT}\right), \quad (2)$$

where z is the charge of the adsorbed ion, F is the Faraday constant (96485 C/mol), R is the universal gas constant (8.314 J/mol K), T is the absolute temperature (K), and Ψ_x is the potential at the plane of adsorption assuming a simple electric double layer, calculated by a one-site, two-pK non-Nernstian model of the surface, i.e.,

$$> SOH_2^+ \leftrightarrow\ > SOH + H_S^+, \quad K_{a1} \quad (3)$$

$$> SOH \leftrightarrow\ > SO^- + H_S^+, \quad K_{a2}, \quad (4)$$
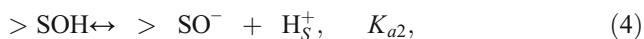
where >S represents the surface of sediment particles, and K_{a1} and K_{a2} are the surface acidity constants. Detailed discussions of Ψ_x refer to Hao et al. (2003) and Supplementary material. The Langmuir model cannot represent the effect of pH on adsorption as it can only fit data obtained at constant pH conditions (Esposito et al. 2002). Thus, a function of pH derived from the experiment data was introduced into Eq. 1 to better simulate the pH effect on P adsorption (Pagnanelli et al. 2003), i.e.,

$$Q = Q_{max}\frac{f\ (pH)\ KC}{1\ +\ KC}. \quad (5)$$

It is worth noting that the adsorption capacity Q_{max} is an ideal value for the maximum P adsorption capacity. Here, the function of $Q_{max}f(pH)$, denoted as q_{max}, is the actual adsorption capacity under different experimental conditions, which is generally smaller than the ideal adsorption capacity.

Surface morphology characterization

Sediment particles have extremely complex surface morphology, which affects pollutants' adsorption significantly. To relate surface morphology to adsorption behaviors, mathematical methods were proposed to characterize the morphology (see Fig. 1). First, the contours of sediment particles were extracted from the scanning electron microscopy images using the edge function of Matlab. Then, Fourier analysis was applied to approximate these contours with the following equation (Fang et al. 2014, 2015):

$$R(\theta) = \overline{R}$$
$$+ \overline{R}\sum_{i\ =\ 1}^{\infty} [a_i\ \cos\ (i\omega\theta)\ +\ b_i\ \sin\ (i\omega\theta)], \quad (6)$$

where R is the polar radius, $\overline{R}$ denotes the average radius, i represents the number of series, arrays of $\{a_i\}$ and $\{b_i\}$ are the Fourier coefficients, ω is the frequency (=$2\pi/T$, T is the period), and θ is the polar angle. Fourier analysis is an effective method to express periodic functions. Previous researches showed that Eq. 6 could effectively simulate sediment particle contours with a high precision when i was not less than 10 (Fang et al. 2014). As shown in Fig. 1, there were significant similarities between the contours of the simulated and original sediment particles, providing evidence for the feasibility of mathematical characterizations. Each contour corresponded to a set of Fourier coefficients, and the statistics of Fourier coefficients were obtained by analyzing a large number of sediment particles, with which a contour of statistical concept was further obtained. Then, a statistical sediment particle was constructed using the statistical contour, exhibiting the overall morphology of sediment particles (Fang et al. 2015).

Based on the Fourier analysis, the external surface area S_{ext} was obtained through the integral of polar radius R over the entire surface, i.e.,

$$S_{ext} = \iint R d\varphi \cdot R\cos\varphi d\theta = 2\overline{R}^2 \cdot T_n, \quad (7)$$
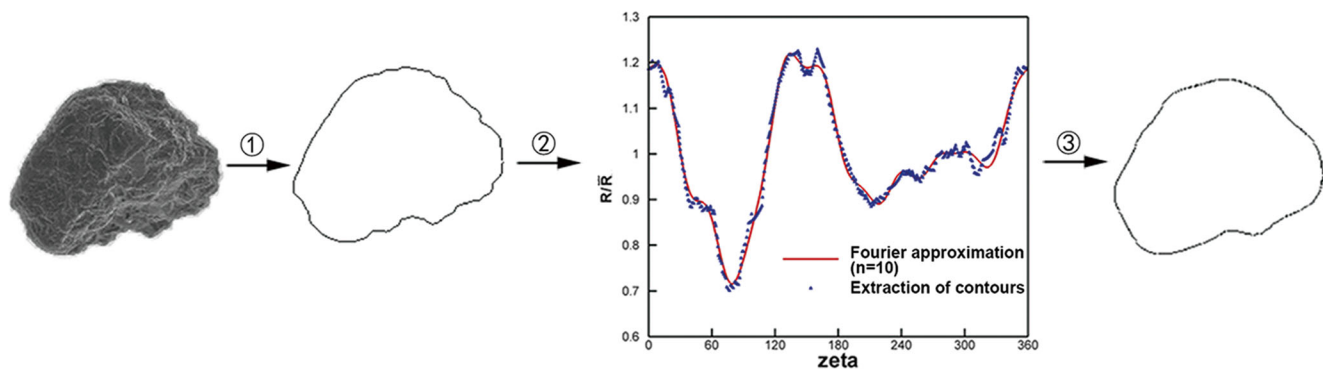

Fig. 1 Fourier analysis of sediment contours (① extracting of contours; ② Fourier approximation; ③ reconstruction of contours)

Table 1 Physical and chemical characteristics of the sediment samples

Samples	Quartz (%)	Microcline (%)	Albite (%)	Muscovite (%)	Clinochlore (%)	Clay (%)	Silt (%)	Sand (%)	D_{50} (μm)
U.L.	81	8	10	1	–	3.1	74.9	22.0	33.1
A.R.	76	4	6	8	6	6.1	65.9	28.0	27.3

Quartz [SiO$_2$], *Microcline* [K(AlSi$_3$)O$_8$], *Albite* [(Na,Ca)Al(Si,Al)$_3$O$_8$], *Muscovite* [KAl$_2$Si$_3$AlO$_{10}$(OH)$_2$], *Clinochlore* [(Mg,Al,Fe)$_6$(Si,Al)$_4$O$_{10}$(OH)$_8$], D_{50} the median diameter

where $T_n = \int_{-\pi}^{\pi} \left\{ 1 + \sum_{i=1}^{\infty} [a_i \cos (i\omega\theta) + b_i \sin (i\omega\theta)] \right\}^2 d\theta$, representing the complexity of surface morphology.

In addition to the complex surface morphology, there are also numerous pores of various dimensions distributed on the surface. All these pores probably increase the potential for pollutants adsorption, exerting great impacts on adsorption properties. According to the BJH theory, the pore size distribution was obtained by the gas adsorption method, i.e., the relation between the change rate of pore volume with respect to pore radius (dV/dr) and the pore radius (r) itself, with which the total pore volume was calculated. If we assumed that all these pores were cylindrical, then the corresponding pore surface area could be expressed as (Barrett et al. 1951)

$$dS_{pore} = 2dV / r. \tag{8}$$

Thus, the total surface area of the pores was calculated through the integral of Eq. 8, i.e.,

$$S_{pore} = \int dS_{pore} = \int \frac{2}{r} \frac{dV}{dr} \, dr. \tag{9}$$

The total surface area of sediment particles, including the areas of both external surface and pores, was then obtained combing Eqs. 7 and 9, i.e., $S = S_{ext} + S_{pore}$. Finally, the adsorption capacity Q_{max}, which was generally treated as a fitting parameter in previous studies, was calculated as a steric close-packed layer of the adsorbed phosphate ions, and introduced into Eq. 5 for the adsorption isotherm simulation.

Results and discussion

Sediment characteristics

The general physical and chemical characteristics of the sediment samples are presented in Table 1. X-ray diffraction analysis illustrated that quartz was the major component of the sediment samples with the percentage of about 80 %. And there was more feldspar for U.L. sediment (i.e., microcline and albite, each accounted for about 10 %), while more clay minerals (i.e., muscovite and clinochlore) for A.R. sediment, which was probably due to the different particle size distributions. Generally, more clay minerals were found in finer sediment. The median diameters D_{50} were 33.1 and 27.3 μm for the U.L. and A.R. sediments, respectively. Meanwhile, the silt fraction was the major fraction in both the sediment samples, and the A.R. sediment possessed a more uniform particle size distribution.

Figure 2 shows the scanning electron microscopy images of the U.L. sediment sample. As shown in the left image, sediment particles had extremely irregular shapes which were different from any simple geometry. Thus, abundant information of surface micro-morphology exist on sediment particles including peak, ridge, channel, pass, pit, and slope, which will affect P adsorption significantly. The local enlarged image shown in the right image provides a better view of the pore structures. There are pores of various dimensions widely distributed on the particle surfaces, ranging from a few nanometers to hundreds of nanometers. Though these pores have different geometries, they were all simplified to be cylindrical in this study.

Fig. 2 Scanning electron microscopy image of the U.L. sediment sample and the local enlarged image
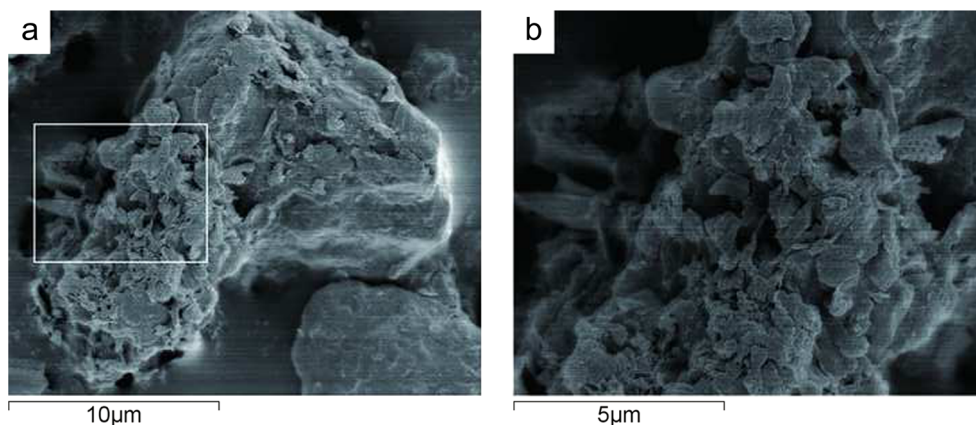
Table 2 Statistics of the Fourier coefficients for both the U.L. and A.R. sediments

Coef.	U.L.		A.R.		Coef.	U.L.		A.R.	
	Avg.	S.D.	Avg.	S.D.		Avg.	S.D.	Avg.	S.D.
a_1	0.004	0.021	0.002	0.018	b_1	0.009	0.020	−0.003	0.019
a_2	−0.016	0.216	0.049	0.136	b_2	−0.013	0.170	−0.015	0.115
a_3	−0.016	0.053	−0.013	0.052	b_3	−0.004	0.066	0.013	0.061
a_4	0.016	0.051	0.006	0.037	b_4	−0.028	0.047	0.010	0.043
a_5	0.005	0.033	−0.005	0.042	b_5	−0.018	0.023	0.004	0.034
a_6	−0.016	0.022	0.003	0.018	b_6	−0.005	0.019	−0.005	0.016
a_7	0.000	0.025	−0.012	0.019	b_7	0.001	0.022	0.005	0.013
a_8	0.002	0.013	−0.005	0.007	b_8	0.003	0.009	−0.003	0.014
a_9	−0.004	0.015	−0.002	0.015	b_9	0.004	0.015	−0.001	0.009
a_{10}	0.003	0.011	−0.001	0.013	b_{10}	−0.001	0.013	−0.001	0.008

Coef. coefficients, *Avg.* average value, *S.D.* standard deviation

We randomly selected 100 sediment particles for Fourier analysis to establish a representative sample space. As stated above, each sediment particle corresponds to a set of Fourier coefficients $\{a_i\}$ and $\{b_i\}$ ($i = 1, \infty$), and the statistics of the Fourier coefficients were obtained by analyzing the 100 sediment particles. Table 2 shows the statistics of the first ten Fourier coefficients for both the U.L. and A.R. sediments, including the average values and standard deviations. Moreover, the box plot of the Fourier coefficients is presented in Fig. 3 for the U.L. sediment, indicating a more significant variation for the coefficients a_2 and b_2 than others. Fang et al. (2015) concluded that the coefficients a_2 and b_2 reflected the elongation degree (or aspect ratio) of sediment particles. Combining the Fourier coefficients and median diameters, the external surface area S_{ext} was then calculated through Eq. 7, i.e., 0.068 and 0.083 m²/g for the U.L. and A.R. sediment, respectively (see Table 3).

The measured pore size distributions are shown in Fig. 4, where the solid circles and hollow triangles represent the U.L. and A.R. sediments, respectively. It was observed that most pores distributed in the range of 20 ~ 500 Å, i.e., mesopore, so the BJH theory was appropriate for the pore structures analysis (Barrett et al. 1951; Groen et al. 2003). The most probable radius for the U.L. and A.R. sediments were similar, i.e., 19.2 and 19.0 Å, respectively, while the A.R. sediment samples had a greater percentage of large pores, which were more prone to adsorb phosphate ions (Horcajada et al. 2004). Similarly, the

total surface area of the pores S_{pore} was calculated using the pore size distribution through Eq. 9, i.e., 7.899 and 11.307 m²/g for the U.L. and A.R. sediment, respectively (see Table 3).

Effects of pH on P adsorption

Adsorption of P by sediments is dependent on pH values (de Jonge et al. 2001; Gimsing et al. 2004). The surface potentials of sediment particles were determined by the protonation and deprotonation of surface hydroxyl groups, i.e., Eqs. 3 and 4, which were directly related to the pH value. Thus, different surface potentials were generally expected with different pH, resulting in different coulombic energies and adsorption equilibrium constants. According to Hao et al. (2003), the calculated adsorption equilibrium constant K was 0.755, 0.432, and 0.424 with pH at 3.65, 4.75, and 5.65, respectively. Here, the surface acidity constants pK_{a1} and pK_{a2} were set at 2.12 and 4.83 for both the U.L. and A.R. sediments according to Wang and Chen (2000). A surface site density of 3.84 μmol/m² was chosen as recommended by Davis and Kent (1990) for bulk composite materials. A decreasing trend of K vs. pH was observed, corresponding to an increasing trend of ΔG_{coul} vs. pH implying a higher affinity of sediment particles to phosphate ions at lower pH values. These variations illustrated the effects of surface charge change on P adsorption due to variations in pH value.

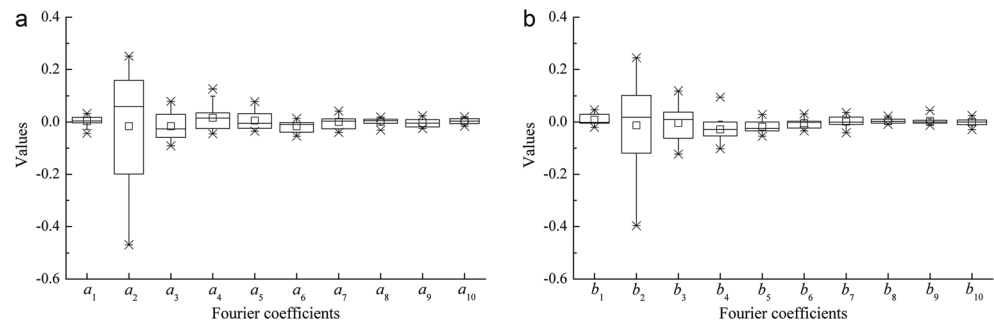**Fig. 3** Box plot of the Fourier coefficients for the U.L. sediment

Table 3 The calculated surface areas of the external surface (S_{ext}) and the pores (S_{pore}), as well as the ideal (Q_{max}) and fitted (q_{max}) P adsorption capacity for the U.L. and A.R. sediments

Samples	S_{ext} (m²/g)	S_{pore} (m²/g)	Q_{max} (mg/g)	q_{max} (mg/g)		
				pH = 3.65	pH = 4.75	pH = 5.65
U.L.	0.068	7.899	0.684	0.636	0.388	0.307
A.R.	0.083	11.307	0.978	0.761	0.648	0.525

Moreover, the adsorption capacity Q_{max}, calculated as a steric close-packed layer of the adsorbed ion, is an ideal value for the maximum P adsorption capacity. The fitted (actual) adsorption capacities under different experimental conditions q_{max} are generally smaller than the ideal adsorption capacity. Table 3 shows the adsorption capacity Q_{max} and the fitted values q_{max} at different pH values. Similar to Pagnanelli et al. (2003), the pH effect on P adsorption was further simulated using an empirical model, and the basic idea was that the experimental relation between q_{max}/Q_{max} and pH could be fitted using an empirical equation, i.e., f(pH) in Eq. 5. It was worth noting that Pagnanelli et al. (2003) directly fitted the experimental relation between q_{max} and pH, while q_{max} was also affected by many other factors besides pH, e.g., the specific surface area. Thus, a relation between q_{max}/Q_{max} and pH should be more appropriate for the adsorption simulation. Here, the power pH functions were selected (see Fig. 5), i.e.,

$$\text{U.L.:} \quad f(\text{pH}) = 2.31\text{pH}^{-0.83}, \quad R^2 = 0.96 \quad (10)$$

$$\text{A.R.:} \quad f(\text{pH}) = 8.08\text{pH}^{-1.68}, \quad R^2 = 0.99. \quad (11)$$

Apparently, the P adsorption capacity of sediment samples decreased significantly with the increasing pH for both the U.L. and A.R. sediments, attributing to the attractive interactions between the negatively charged phosphate ions and the positively charged surface at low pH (i.e., $>\text{SOH}_2^+$). It was observed that the fitted P adsorption capacity was close to the

ideal one at pH 3.65, while it was only about half of the ideal capacity at pH 5.65, implying the significant change in reactive surface area for P adsorption. Moreover, the empirical function decreased much more sharply with the increasing pH for the U.L. sediment, indicating a more significant pH effect on P adsorption than for the A.R. sediment. In other words, a more stable P adsorption occurred for the A.R. sediment. Keep in mind that the parameters of power pH functions might not be readily transferrable to other systems and may have to be evaluated to each adsorbent separately.

P adsorption with different pH

The results of P adsorption by the U.L. and A.R. sediments with different pH are shown in Fig. 6. First, the adsorption increased linearly at low P equilibrium concentration. Then, the increase rate gradually decreased with increase in P concentration. Generally, the P adsorption amount with different pH was as follows: pH = 3.65 > pH = 4.75 > pH = 5.65, i.e., more P adsorbed at lower pH values, indicating a monotonically decreasing relation with pH values. The reduced P adsorption at higher pH was most likely due to the absence of $>\text{SOH}_2^+$ and the formation of $>\text{SO}^-$ at higher pH (Zheng et al. 2012). Overall, the A.R. sediment had a stronger adsorption capacity at the same pH compared to the U.L. sediment. According to the sediment characterizations, the A.R. sediment had more clay minerals, smaller median diameter, and a greater
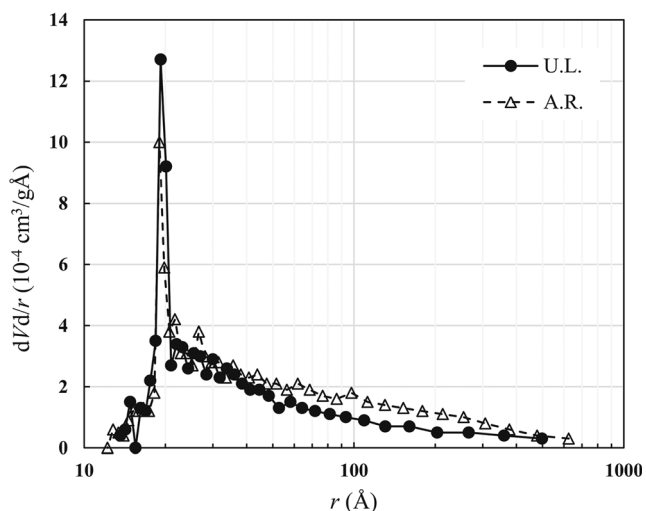

Fig. 4 Differential pore size distributions for both the U.L. and A.R. sediment samples
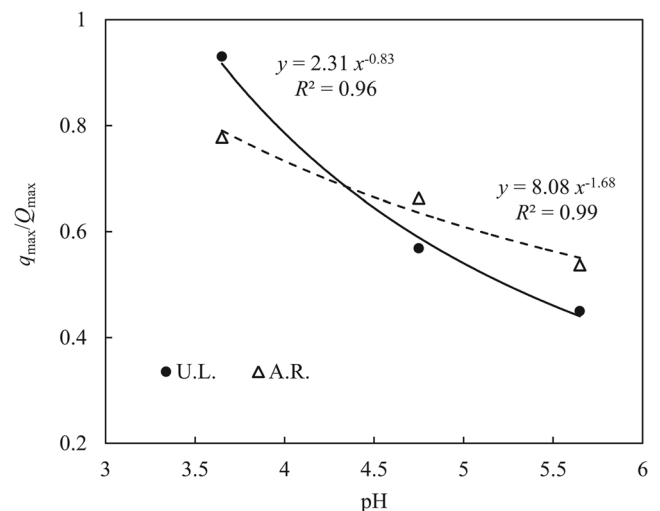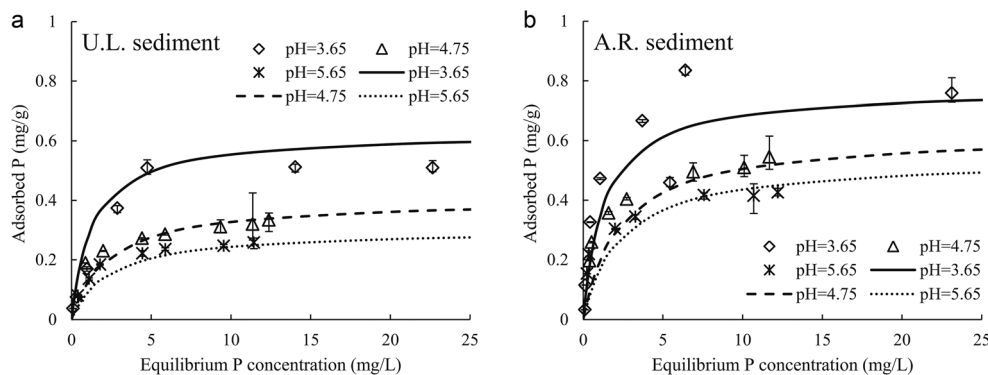

Fig. 5 Experimental relations between q_{max}/Q_{max} and pH for the U.L. and A.R. sediment samples

Fig. 6 The measured and simulated P adsorption by the U.L. and A.R. sediments with different pH

percentage of large pores than the U.L. sediment. Clay minerals contributed to a large portion of the Fe/Al contents, which had a high affinity for the phosphate ions (Danen-Louwerse et al. 1993; Wang et al. 2009). Particle size distribution was an important factor affecting P adsorption at the solid-water interface (Wang et al. 2006). Finer grain fractions provided most of the sediment particle surface and had a larger P adsorption capacity. According to the surface morphology and pore size distribution, the A.R. sediment has a larger specific surface area exerting a dominant role in the P adsorption. The estimated adsorption capacity Q_{max} for the A.R. sediment was approximately 40 % percent greater than the U.L. sediment.

Substituting Eqs. 10 and 11 into Eq. 5, we obtained the adsorption models for the U.L. and A.R. sediment respectively. The simulated results are presented in Fig. 6. There was no fitting parameter in the adsorption isotherms except the empirical power pH functions, and both the adsorption capacity Q_{max} and adsorption equilibrium constant K were theoretically derived. In Fig. 6, the solid, dashed, and dotted lines represented the adsorption isotherms at pH 3.65, 4.75, and 5.65, respectively. Overall, the simulated adsorption isotherms were in good agreement with the measurements, which well reproduced the pH effect on P adsorption for both the U.L. and A.R. sediments. The normalized root mean square errors (NRMSE) of the adsorbed P for the U.L. sediment were 0.172, 0.125, and 0.165 at pH .65, 4.75, and 5.65, respectively, and the values were 0.257, 0.212, and 0.228 for the A.R. sediment. To establish an intuitive feeling of the performance of the proposed model, the measured and simulated values of the adsorbed P are further compared in Fig. 7 for all pH, where x-axis and y-axis represent the measured and simulated values, respectively. In Fig. 7, the solid line indicates that the simulated values are equal to the measured values, i.e., $y = x$, and it was observed that the simulated results were generally close to the line of perfect agreement. However, the simulation slightly underestimated the P adsorption amount of the A.R. sediment, while a relatively better simulation was achieved for the U.L. sediment, which is probably due to the more significant fluctuation of the measured P adsorption for the A.R. sediment (see Fig. 6).

In this study, the adsorption capacity Q_{max} was calculated as a steric close-packed layer of the adsorbed ions, i.e., all the

surface micro-morphology was treated equally. The affinity to phosphate ions varied among different surface micro-morphology (Fang et al. 2013), and P adsorption by sediment particles significantly depends on the surface morphology. The complex surface morphology probably resulted in surface charge heterogeneities, i.e., nonuniform surface charge distribution, which would result in different adsorption potential on each local adsorption site affecting the interactions between sediment particles and phosphate ions (Huang et al. 2012). Nevertheless, the surface potential was simply calculated based on the assumption of smooth surface and uniform surface charge distribution to derive the adsorption equilibrium constant. Moreover, the pores of various dimensions also exerted great impacts on adsorption properties. Previous research showed that the average pore size and total pore volume of sediment particles decreased after P adsorption (Fang et al. 2008), and the adsorption properties varied among different pore sizes (Pelekani and Snoeyink 1999). Solutes had a tendency to adsorb onto more active sites (Sohn and Kim 2005). The existence of these surface heterogeneities would lead to the heterogeneous adsorption on the sediment particle
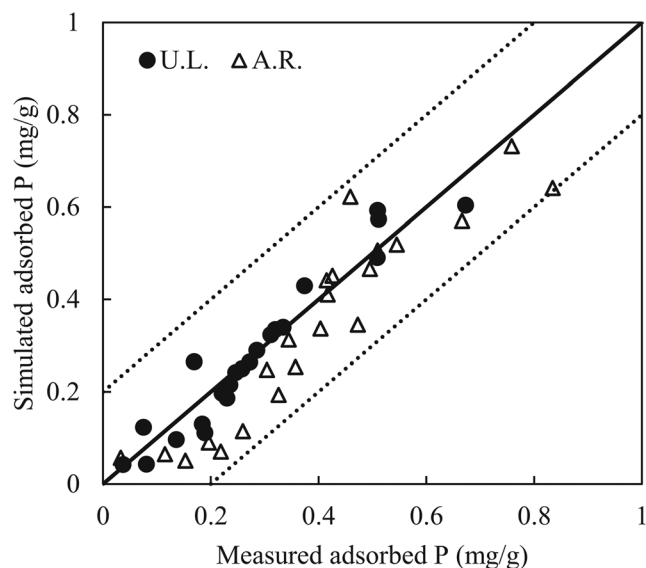

Fig. 7 Comparison between the measured and simulated P adsorption by the U.L. and A.R. sediments

surfaces. As shown in Fig. 6, the P adsorption was enhanced with lower pH, and an empirical function of pH was introduced to represent the pH effect on P adsorption. However, from this simple function, it is difficult to comprehensively reflect on the complexity of surface morphology resulting in discrepancies between the P simulations and measurements (see Fig. 7). Thus, it is essential to further study the P adsorption mechanisms by considering the complex surface morphology and pore structures more comprehensively.

Conclusions

In this paper, P adsorption by the U.L. and A.R. sediment samples was studied with different pH values. The surface morphology of sediment samples were observed using a scanning electron microscopy and approximated by the Fourier analysis. The pore structures, including the pore volume and pore size distribution, were characterized by a gas adsorption method. For simplification, all the pores were assumed to be cylindrical. The ideal adsorption capacity was then estimated by assuming a steric close-packed layer of the adsorbed phosphate ions, and an empirical function of pH was further introduced to represent the pH effect on P adsorption. The relative smaller value of the actual adsorption capacity indicated the importance of deriving the P-reactive surface area under experimental conditions. The adsorption equilibrium constant was derived based on a one-site, two-pK non-Nernstian model of the surface. It was observed that the more clay minerals, smaller median diameter, and a greater percentage of large pores resulted in a stronger P adsorption for the A.R. sediment. The P adsorption capacity, as well as the adsorption equilibrium constant, decreased with increasing pH, most likely due to the absence of $>SOH_2^+$ at higher pH and the corresponding surface charge change. These phenomena were well simulated by the adsorption isotherms. Sediment particles have extremely complex morphology, which affects P adsorption significantly. The affinity to phosphate ions varies among different surface micro-morphology, and further researches are still required to consider the adsorption properties of various micro-morphology thoroughly.

References

Antelo J, Avena M, Fiol S, López R, Arce F (2005) Effect of pH and ionic strength on the adsorption of phosphate and arsenate at the goethite-water interface. J Colloid Interf Sci 285:476–486

Barrett EP, Joyner LG, Halenda PP (1951) The determination of pore volume and area distributions in porous substances. I. Computations from nitrogen isotherms. J Am Chem Soc 73:373–380

Brandt RK, Hughes MR, Bourget LP, Truszkowska K, Greenler RG (1993) The interpretation of CO adsorbed on Pt/SiO2 of two different particle-size distributions. Surf Sci 286:15–25

Danen-Louwerse H, Lijklema L, Coenraats M (1993) Iron content of sediment and phosphate adsorption properties. Hydrobiologia 253:311–317

Davis JA, Kent DB (1990) Surface complexation modeling in aqueous geochemistry. Rev Mineral Geochem 23:177–260

de Jonge H, de Jonge LW, Jacobsen OH, Yamaguchi T, Moldrup P (2001) Glyphosate sorption in soils of different pH and phosphorus content. Soil Sci 166:230–238

Elser JJ, Bracken MES, Cleland EE, Gruner DS, Harpole WS, Hillebrand H, Ngai JT, Seabloom EW, Shurin JB, Smith JE (2007) Global analysis of nitrogen and phosphorus limitation of primary producers in freshwater, marine and terrestrial ecosystems. Ecol Lett 10:1135e1142

Esposito A, Pagnanelli F, Vegliò F (2002) pH-related equilibria models for biosorption in single metal systems. Chem Eng Sci 57:307–313

Fang HW, Chen MH, Chen ZH (2008) Analysis of polluted sediment surface pore tension and adsorption characteristics. Sci China, Ser G 51:1022–1028

Fang HW, Chen MH, Chen ZH, Zhao HM, He GJ (2013) Effects of sediment particle morphology on adsorption of phosphorus elements. Int J Sediment Res 28:246–253

Fang HW, Chen MH, Chen ZH, Zhao HM, He GJ (2014) Simulation of sediment particle surface morphology and element distribution by the concept of mathematical sand. J Hydro-environ Res 8:186–193

Fang HW, Zhao HM, Chen ZH, Chen MH, Zhang YF (2015) 3D shape and morphology characterization of sediment particles. Granul Matter 17:135–143

Fang HW, Lai RX, Lin BL, Xu XY, Zhang FX, Zhang YF (2016) Variational-based data assimilation to simulate sediment concentration in the Lower Yellow River, China. J Hydrol Eng 21:04016010

Gimsing AL, Borggaard OK, Bang M (2004) Influence of soil composition on adsorption of glyphosate and phosphate by contrasting Danish surface soils. Eur J Soil Sci 55:183–191

Goldberg S, Sposito G (1984) A chemical model of phosphate adsorption by soils: II. Noncalcareous soils. Soil Sci Soc Am J 48:779–783

Groen JC, Peffer LA, Pérez-Ramírez J (2003) Pore size determination in modified micro-and mesoporous materials. Pitfalls and limitations in gas adsorption data analysis. Micropor Mesopor Mat 60:1–17

Han BC, Miranda CR, Ceder G (2008) Effect of particle size and surface structure on adsorption of O and OH on platinum nanoparticles: a first-principles study. Phys Rev B 77:075410

Hao X, Spieker WA, Regalbuto JR (2003) A further simplification of the revised physical adsorption (RPA) model. J Colloid Interf Sci 267:259–264

Hong YS, Kinney KA, Reible DD (2011) Effects of cyclic changes in pH and salinity on metals release from sediments. Environ Toxicol Chem 30:1775–1784

Horcajada P, Ramila A, Perez-Pariente J, Vallet-Regı M (2004) Influence of pore size of MCM-41 matrices on drug delivery rate. Micropor Mesopor Mat 68:105–109

Huang L, Fang HW, Chen MH (2012) Experiment on surface charge distribution of fine sediment. Sci China Ser E 55:1146–1152

Huang L, Fang HW, Reible DD (2015) Mathematical model for interactions and transport of phosphorus and sediment in the Three Gorges Reservoir. Water Res 85:393–403

Iqbal J, Shah MH, Shaheen N (2015) Distribution, source identification and risk assessment of selected metals in sediments from freshwater lake. Int J Sediment Res 30:241–249

Johnson BB (1990) Effect of pH, temperature, and concentration on the adsorption of cadmium on goethite. Environ Sci Technol 24:112–118

Olsen SR, Watanabe FS (1957) A method to determine a phosphorus adsorption maximum of soils as measured by the Langmuir isotherm. Soil Sci Soc Am J 21:144–149

Pagnanelli F, Esposito A, Toro L, Vegliò F (2003) Metal speciation and pH effect on Pb, Cu, Zn and Cd biosorption onto *Sphaerotilus natans*: Langmuir-type empirical model. Water Res 37:627–633

Palleyi S, Banoo S, Kar RN, Panda CR (2015) Textural and geochemical characteristics of off shore sediment of North Bay of Bengal: a statistical approach for marine metal pollution. Int J Sediment Res 30:208–222

Pelekani C, Snoeyink VL (1999) Competitive adsorption in natural water: role of activated carbon pore size. Water Res 33:1209–1219

Rodda DP, Johnson BB, Wells JD (1996) Modeling the effect of temperature on adsorption of lead (II) and zinc (II) onto goethite at constant pH. J Colloid Interf Sci 184:365–377

Schindler DW (2006) Recent advances in the understanding and management of eutrophication. Limnol Oceanogr 51:356e363

Selig U (2003) Particle size-related phosphate binding and P-release at the sediment-water interface in a shallow German lake. Hydrobiologia 492:107–118

Shen ZL (2006) Phosphorus and silicate fluxes in the Yangtze River. Acta Geogr Sinica 61:741–751, in Chinese

Sohn S, Kim D (2005) Modification of Langmuir isotherm in solution systems—definition and utilization of concentration dependent factor. Chemosphere 58:115–123

Venkatramanan S, Chung SY, Ramkumar T, Gnanachandrasamy G, Kim TH (2015) Evaluation of geochemical behavior and heavy metal distribution of sediments: the case study of the Tirumalairajan river estuary, southeast coast of India. Int J Sediment Res 30:28–38

Wang FY, Chen JS (2000) Preliminary research on surface properties of river surface sediment in eastern China. Acta Scien Circum 20:682–687 (in Chinese)

Wang SR, Jin XC, Bu QY, Zhou XN, Wu FC (2006) Effects of particle size, organic matter and ionic strength on the phosphate sorption in different trophic lake sediments. J Hazard Mater 128:95–105

Wang Y, Shen ZY, Niu JF, Liu RM (2009) Adsorption of phosphorus on sediments from the Three-Gorges Reservoir (China) and the relation with sediment compositions. J Hazard Mater 162:92–98

Wang XY, Zhang LP, Zhang HS, Wu XY, Mei DL (2012) Phosphorus adsorption characteristics at the sediment-water interface and relationship with sediment properties in FUSHI reservoir, China. Environ Earth Sci 67:15–22

Yan F, Chu YY, Zhang K, Zhang FF, Bhandari N, Ruan GD, Dai ZY, Liu Y, Zhang Z, Kan AT, Tomson MB (2015) Determination of adsorption isotherm parameters with correlated errors by measurement error models. Chem Eng J 281:921–930

Yu KC, Tsai LJ, Chen SH, Ho ST (2001) Correlation analyses on binding behavior of heavy metals with sediment matrices. Water Res 35:2417–2428

Zhao Y, Yang S, Li HH, Wang D (2015) Adsorption behaviors of acetaminophen onto sediment in the Weihe River, Shaanxi, China. Int J Sediment Res 30:263–271

Zheng TT, Sun ZX, Yang XF, Holmgren A (2012) Sorption of phosphate onto mesoporous γ-alumina studied with in-situ ATR-FTIR spectroscopy. Chem Cent J 6:26